

# 1 Landscape expressions of tectonics in the Zagros fold-and-thrust belt

2  
3 Ahmed K. Obaid <sup>1,2</sup>, Mark B. Allen <sup>2</sup>

4 <sup>1</sup> Department of Geology, University of Baghdad, Al-Jadriyh Street, Baghdad, Iraq

5 <sup>2</sup> Department of Earth Sciences, University of Durham, Durham DH1 3LE, UK

6 ahamedobaid@gmail.com; m.b.allen@durham.ac.uk

## 7 8 **Abstract**

9  
10 This study uses geomorphic indices, including normalized channel steepness index ( $k_{sn}$ ),  
11 integrated relief and hypsometric index (HI), to investigate how landscape responds to  
12 tectonic and climatic drivers in the Zagros fold-and-thrust belt, and show how geomorphology  
13 can be a sensitive indicator of tectonic processes. There is a broad association of relatively  
14 high  $k_{sn}$  values ( $>50 \text{ m}^{0.9}$ ) with the upper elevation limit for seismogenic thrusting, which  
15 occurs regionally at the 1250 m topographic contour. Higher  $k_{sn}$  values occur beyond this  
16 seismicity cut-off in the Bakhtyari Culmination, but are rare in the Fars region. We measured  
17 HI values for 17380 third order river basins across the Zagros. In many areas the low/high HI  
18 transition (0.3) is typically at the elevation limit of seismogenic thrusting. There are two  
19 important exceptions. In the Dezful Embayment/Bakhtyari Culmination the low/high HI  
20 transition lies at higher elevations than the thrust seismicity cut-off. In the Fars region, the HI  
21 transition lies at lower elevations than the seismicity cut-off. We explain these differences by  
22 the different climates of the two areas: wetter conditions and vigorous drainage systems in the  
23 Dezful/Bakhtyari region retard orogenic plateau growth; drier climate and low power rivers in  
24 the Fars region promote plateau growth. Orographic precipitation may itself have a tectonic  
25 control; regional basement strength variations have caused intense thrusting and high relief in  
26 the Bakhtyari Culmination. Integrated relief of five across-strike Zagros topographic swath  
27 profiles is in the range  $2.2 - 2.8 \cdot 10^8 \text{ m}^2$ . We argue that this consistency within  $\sim 25\%$  relates to  
28 the comparable strain rates across different sectors of the Zagros, regardless of local  
29 structural, drainage network or climatic variations.

## 30 **1. Introduction**

31 The tectonics of the Zagros are far from completely understood, despite it being one of the  
32 largest and most active fold-and-thrust belts on Earth (Fig. 1). Information in the present  
33 landscape has not been fully analysed to improve tectonic models. Nor do we understand the  
34 interactions of landscape, tectonics and climate. In this study we have conducted a range-wide

35 analysis of geomorphology to improve the current state of knowledge of Zagros tectonics. We  
36 hypothesise that geomorphic and structural variations between different regions of the range  
37 might correlate with variations in climate, but that the climatic variations might ultimately be  
38 controlled by the pre-collisional, basement geology of the Zagros.

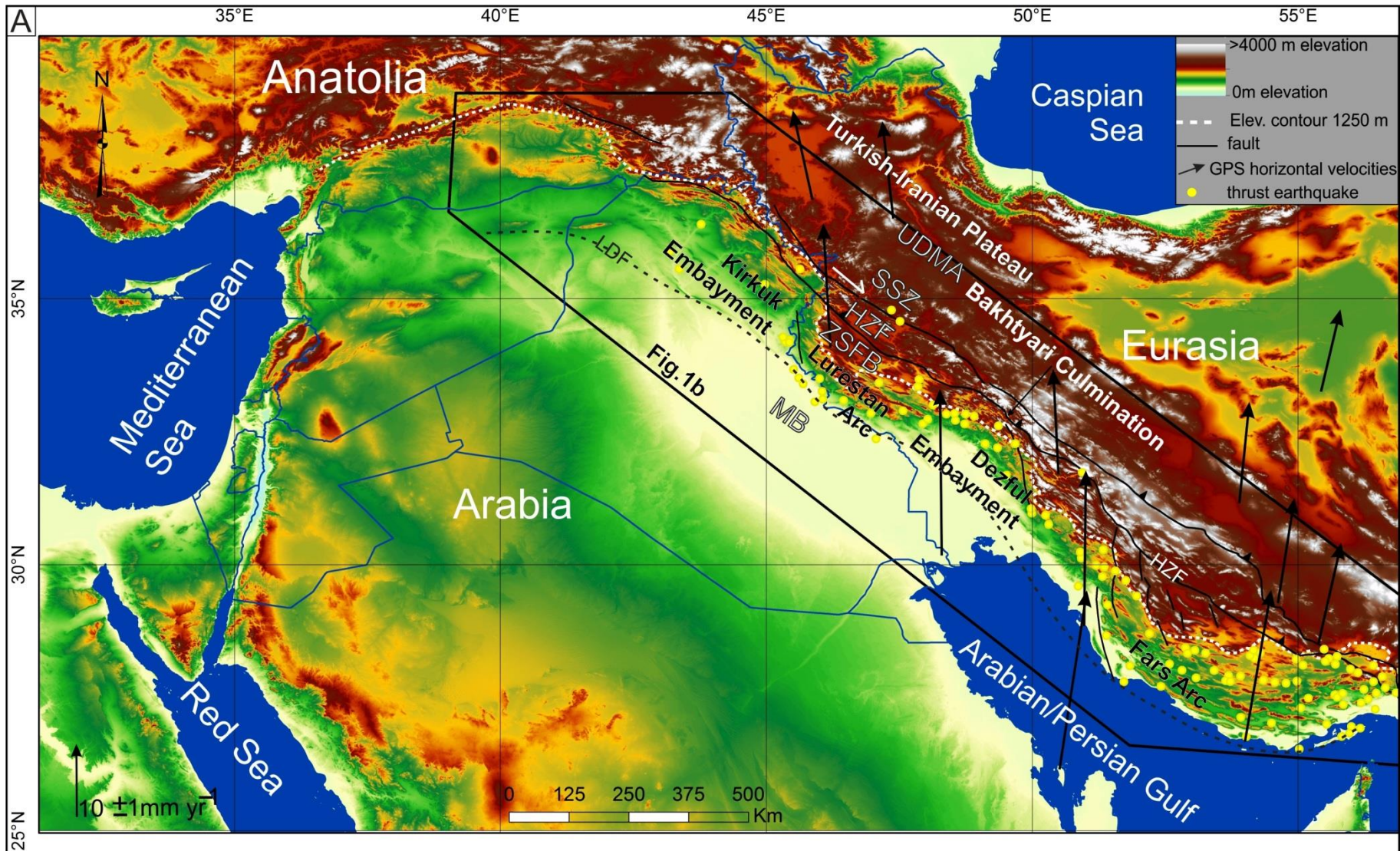
39 One of the major tectonic events of the Cenozoic was the closure of the Neo-Tethys Ocean. A  
40 consequence of this closure was the Arabia-Eurasia collision, which initiated the Zagros fold-  
41 and-thrust belt as one of the largest and most tectonically active mountain ranges in the world  
42 (Mouthereau et al., 2012). It has accommodated part of the Arabia-Eurasia convergence  
43 (Blanc et al. 2003; McQuarrie, 2004; Ghasemi and Talbot, 2006; Alavi, 2007) since at least  
44 the Early Miocene (Fakhari et al., 2008; Khadivi et al., 2010; Khadivi et al., 2012). The  
45 Zagros fold-and-thrust belt deforms both the underlying basement and the overlying folded  
46 sedimentary cover of the Arabian Plate (Talebian and Jackson, 2004). The Zagros represents  
47 an area with a wide range of exposed geology, but mainly sedimentary rocks from the Jurassic  
48 to the Holocene (Fig. 1b).

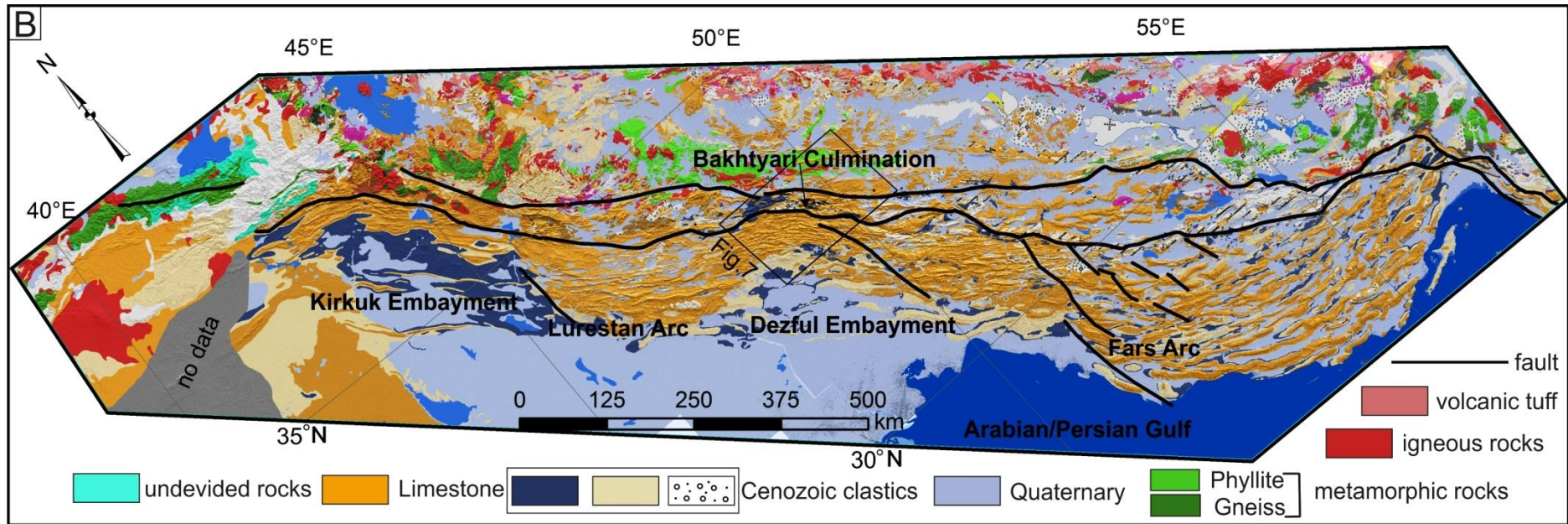
49 Whereas there is pronounced crustal deformation within the Zagros, shown by the abundant  
50 seismicity and shortening across the range, the Turkish-Iranian Plateau represents a region of  
51 the collision zone where there is little active convergence, relatively low relief, and subdued  
52 seismicity (mainly strike-slip) (Nissen et al., 2011). The boundary between the plateau and the  
53 active fold-and-thrust belt is debatable, but there is a marked cut-off in thrust seismicity at the  
54 1250 m elevation contour (Fig. 1a). Most thrust events are confined to the low elevation part  
55 of the Zagros Simply Folded Belt, below the 1250 m elevation contour (Nissen et al., 2011).  
56 Elevations continue to climb to the northeast, but with little indication of active shortening, at  
57 least at upper crustal levels (Allen et al., 2013). The thrust seismicity cut-off is therefore an  
58 important marker for studies of landscape response to tectonism in the Zagros.

59 Active tectonism has been widely investigated using multiple geomorphic indices because of  
60 their ability to detect the landscape response to tectonic drivers (e.g. Lavé and Avouac, 2000;  
61 Keller and Pinter, 2002; Zielke et al., 2010). In addition, these indices provide measurements  
62 which help assess the relative roles of crustal displacement and the variation in rock resistance  
63 during landscape development (e.g. Walcott and Summerfield, 2008).

64 The study of river-fold interaction in the Zagros has previously been dealt with by local  
65 studies in different parts of the Zagros (e.g. Bahrami, 2013; Bretis et al., 2011; Burberry et al.,  
66 2008, 2010; Ramsey et al., 2008; Walker et al., 2011; Zebari and Burberry, 2015; Obaid and

67 Allen, 2017). This paper studies the regional landscape response of the Zagros to potential  
68 climatic and tectonic drivers. The geomorphic indices used are: hypsometric index (HI) of  
69 drainage basins,  $k_{sn}$  values, and the integrated topographic relief for across-strike topographic  
70 swath profiles.





72

73 Fig.1. Regional topography, tectonics and lithologies of the Zagros fold-and-thrust belt. (a) Tectonic division zones after Berberian (1995), GPS  
 74 velocities (stable Eurasia reference frame) after Vernant et al., 2004. UDMA = Urumieh-Dokhtar Magmatic Arc; SSZ = Sanandaj-Sirjan Zone;  
 75 HZF = High Zagros Folds; ZSFB = Zagros Simply Fold Belt; LDF = Limit of Deformation Front; MB = Mesopotamian Basin. (b). Exposed  
 76 lithologies of the Zagros fold-and-thrust belt (redrawn after (1) the geological map of Turkey 1:2,000,000; (2) Sissakian, 2000 and (3) Afaghi and  
 77 Salek, 1975a; 1975b; 1977a; 1977b; 1977c; Afaghi et al., 1978).

78

## 79 **1.1. Regional Zagros geology**

80 The Zagros region has been subjected to a series of compressional and extensional phases  
81 during its geological history that have initiated and later reactivated a series of basement  
82 faults (Ameen 1992; Jassim and Goff 2006; Stern and Johnson 2010; Lacombe et al., 2011;  
83 Burberry 2015). The Arabia-Eurasia collision is only the latest of these events. The Zagros  
84 fold-and-thrust belt is built over what was the northern, passive continental margin of the  
85 Arabian Plate before its initial collision with Eurasia. Initial collision may have been roughly  
86 at the Eocene-Oligocene boundary (~35 Ma, Allen and Armstrong 2008; Perotti et al., 2016)  
87 or in the Late Oligocene-Early Miocene (~27-23 Ma, Mouthereau et al., 2012; McQuarrie and  
88 van Hinsbergen, 2013). The present Zagros fold-and-thrust belt (Fig. 1a) passes through the  
89 north and northeast of Iraq, across southern Iran and ends at ~57° E where it juxtaposes the  
90 Makran accretionary complex (Mouthereau et al., 2006; Alavi 2007). GPS data suggests that  
91 the region accommodates a northward movement of the Arabian Plate at a rate of ~16-26  
92 mm/yr (Vernant et al. 2004), with the convergence rate increasing eastwards.

93 The Zagros orogen consists of three main parallel tectonic units (Fig. 1a). From the northeast  
94 to the southwest these units are the subduction-related Urumieh-Dokhtar Magmatic Arc, the  
95 Sanandaj-Sirjan Zone and the Zagros fold-and-thrust belt.

96 Many folds have developed as a consequence of the Arabia-Eurasia collision. These are the  
97 classic “whaleback” structures of the Zagros fold-and-thrust belt, which trend NW-SE along  
98 the greater part of the range. Anticlines in the north western part of the Zagros (north of ~36°  
99 N) and in the Fars region in the SE have more E-W trends (Fig.1). The High Zagros Fault  
100 separates the High Zagros folds to the north from the Simply Folded Belt to the south. Other  
101 structural divisions have been described across the strike of the orogen, but these are  
102 secondary, and bounded by features such as the Mountain Front Fault that may not be  
103 continuous along the length of the range (Fig.1).

104 Along the strike of the Zagros there are variations in the degree of exhumation, topographic  
105 elevation, relief, stratigraphy, position of the deformation front and structural style changes  
106 along strike (Talbot and Alavi, 1996). These along-strike changes divide the range into  
107 several domains, referred to as salients and embayments, adjacent to the higher elevation  
108 Turkish-Iranian Plateau to the northeast (Fig.1). These domains are the Kirkuk Embayment,  
109 Lurestan (Pusht-e Kuh) Arc, Dezful Embayment and Fars Arc, from the northwest to  
110 southeast (Berberian 1995; Lacombe et al., 2006; Mouthereau et al., 2007; Casciello et al.,

111 2009). The southwestern margins of the Kirkuk and Dezful embayments form a roughly linear  
112 deformation front, separated by the Lurestan/Pusht-e Kuh Arc (salient). To the southeast, the  
113 Fars Arc forms a curved deformation front, convex to the south. There are differences in the  
114 strain distribution within the Zagros related to the occurrence of the embayments (e.g. low  
115 strain in the Dezful Embayment complemented by high strain in Bakhtyari Culmination)  
116 (McQuarrie, 2004; Allen and Talebian, 2011). The origin of the Dezful Embayment has been  
117 related to the pre-continental collision of the Arabian Plate margin, and the irregular  
118 distribution of Cretaceous ophiolites upon it (Allen and Talebian 2011). It is not clear whether  
119 this model applies to the Kirkuk Embayment, however.

120 The boundary between the Simply Folded Belt and the Mesopotamian Foreland Zone is the  
121 current Zagros deformation front, although subtle Cretaceous-Cenozoic structures appear to  
122 the south of this line (including oil and gas fields). The pre-collisional significance of the  
123 boundary is unclear, but likely relates to differences in the Palaeozoic-Mesozoic rifting  
124 history of the Arabian Plate, associated with the opening of Tethys. The “Unstable” and  
125 “Stable” terms in stratigraphic descriptions (e.g. Jassim and Goff, 2006) relate to the  
126 differences began in the pre-Cenozoic, pre-collisional, history and stratigraphy.

127 Because the Zagros fold-and-thrust **belt** is built on the original passive continental margin of  
128 the Arabian Plate, the great majority of exposed rocks are sedimentary, and belong either to  
129 pre- or post-collisional sequences. Total sedimentary thickness commonly exceeds 10 km.  
130 Palaeozoic strata are rarely exposed. Precambrian basement occurs as fragments brought up  
131 by diapirs of the Hormuz Series salt, itself of latest Precambrian-Cambrian age. Carbonates  
132 occur at various levels within the stratigraphy, with important units in the Cretaceous  
133 (Bangestan Group) and mid Tertiary (Asmari Limestone and equivalents). Later Tertiary and  
134 Quaternary units are predominantly clastic, generally coarsen upwards and reveal the foreland  
135 propagation of deformation (Ruh et al., 2014). In terms of erodibility (Moosdorf et al., 2018),  
136 the carbonate units are particularly resistant, and commonly preserve the morphology of  
137 anticlines. Later Cenozoic clastic units are less resistant, and are more commonly preserved in  
138 synclines that are topographic lows between the anticlines. Within the Late Cenozoic clastics  
139 there are evaporites within the Gachsaran Formation and marl in the Mishan and Aghajari  
140 formations.

141 The climate of the Zagros is classified as arid to semi-arid with hot dry summers and cold dry  
142 winters (Kottke et al., 2006). The interaction between the Mediterranean and Sudan Lows

143 synoptic systems with different elevations across the Zagros Mountains produces precipitation  
144 variability in space and time (Boroujerdy et al., 2013).

## 145 **2. Methods and data**

### 146 **2.1. Climate**

147 Rainfall data from the Tropical Rainfall Measuring Mission satellite TRMM 3B43  
148 (<https://mirador.gsfc.nasa.gov/>) were analysed for the time series 1998-2016 (resolution  
149  $0.25^{\circ} \times 0.25^{\circ} \sim 25 \times 25$  km) to allow investigation of first order precipitation variations on  
150 geomorphic indices (Section 3.1), and broader interactions with tectonics.

### 151 **2.2. Topographic swath profiles**

152 Swath profiles represent continuous changes of surface altitude along the swath by maximum,  
153 mean and minimum elevations across the swath width. The general pattern of a landscape can  
154 be represented by the mean elevation. The difference between the maximum and the  
155 minimum elevations is the relief (Molin et al., 2004; Scotti et al., 2014) (also called incision  
156 by Andreani et al., 2014; although there is no requirement that a previous surface is incised).

157 Twenty-five swath profiles oriented NE-SW have been analysed (supplementary figure 1),  
158 using the Shuttle Radar Topography Mission (SRTM) 30 dataset  
159 (<https://www2.jpl.nasa.gov/srtm/>) (30 m pixel size). The width of swaths is 25 km on either  
160 side of the swath centre. Across-profile relief values were integrated to give an indication of  
161 overall relief for the range within each profile area. This is the first time this relief integration  
162 approach has been applied to the regional tectonic geomorphology of a fold-and-thrust belt, as  
163 far as we are aware. Therefore the Zagros system is something of a test case. The intention is  
164 to see what variation there is along the strike of the range, bearing in mind differences in the  
165 structure and climate, as well as any other potential variables.

166

### 167 **2.3. Normalized river-channel steepness ( $k_{sn}$ ) analysis**

168 Features of active deformation can be recognised using the sensitivity of river profiles to  
169 uplift processes (Seeber and Gornitz, 1983). Tectonic geomorphology methods include the  
170 analysis of steady state river long profiles (e.g., Kirby et al., 2003; Snyder et al., 2000;  
171 Whipple and Tucker, 1999; Wohl and Merritt, 2001) or methods which recognise a change in  
172 base level (e.g., Boulton and Whittaker, 2009; Whipple, 2004; Whipple and Tucker, 1999,

173 2002; Whittaker and Boulton, 2012; Whittaker et al., 2007, 2008). Changes in the slope of  
174 river profiles can be recognized by the occurrence of knickpoints, both in slope-area or  
175 elevation-distance plots. Knickpoints can develop in response to tectonic effects (i.e. uplift  
176 caused by folding and/or faulting), or changes in base level (Goldrick and Bishop, 2007;  
177 Kirby and Whipple, 2012; Wobus et al., 2006), among other causes. Knickpoint distribution  
178 has been used to identify tectonic forcing in active orogens (Miller et al., 2012; Schildgen et  
179 al., 2012; Morell et al., 2012; Olivetti et al., 2012).

180 Tucker and Whipple (2002) and Whipple and Tucker (2002) described fluvial erosion in three  
181 conditions. These conditions are 1) detachment-limited models, which represent bedrock  
182 rivers where erosion is equal to uplift, and where a fall in base level or regional uplift and  
183 substrate erodibility control the gradient of river. 2) Transport-limited models, where channel  
184 gradient is determined by the capability of a river to transfer sediment. These cases are  
185 alluvial rivers. 3) The third case is hybrid river models, where substrate erodibility and  
186 sediment flux control the gradient of a channel. A dynamic equilibrium is required between  
187 two competitive parameters; the rate of rock uplift and the rate of terrain removal to preserve  
188 tectonic signals in the landforms (Dietrich et al., 2003).

189 The relationship between local slope of river channel ( $S$ ) and upstream area ( $A$ ) in the form of  
190 a power law (Hack's law) (Hack, 1957; Flint, 1974).

$$191 \quad S = k_s A^{-\theta} \quad (1)$$

192 Where  $k_s$  and  $\theta$  are the steepness index and concavity index, respectively. Slope-area plots  
193 allow the extraction of both  $S$  and  $A$  directly from DEMs using the regression of slope and  
194 area data. Accordingly, the concavity index,  $\theta$ , and the steepness index,  $k_s$ , can be calculated.  
195 The concavity index ( $\theta$ ) in Eq. (1) describes the change in slope along a graded river profile  
196 (Wobus et al., 2006). Significant deviation from a theoretical graded profile, with a smooth  
197 concave-up shape, reflects transient response to changes in tectonic rates (Boulton and  
198 Whittaker, 2009; Snyder et al., 2000; Larue, 2008), rock structures and their resistance  
199 differences (Larue, 2008; Phillips and Lutz, 2008) or other changes in base level and  
200 landscape (Bowman et al., 2007; Harmar and Clifford, 2007). Although the concavity index  
201 shows significant variability in natural streams, in a steady state it often has a value within the  
202 range  $\sim 0.4$ - $0.6$  (Kirby and Whipple, 2001; Snyder et al., 2000; Whipple, 2004; Wobus et al.,  
203 2006). A steady state condition means that there is a balance between erosion and surface

204 uplift. This uniformity leads to the insensitivity of the concavity index to the factors  
205 mentioned above. In contrast, the steepness index exhibits changes in value along the  
206 segmented profile, dependent on these factors. The steepness index incorporates the change in  
207 channel slope and drainage area, to deal with systematic variations in river gradient index as a  
208 result of changes in basin shape and discharge (Goldrick and Bishop, 2007).

209 To overcome the dependence of longitudinal profiles on the basin shape, a linear regression of  
210 gradient against drainage area should be applied on a log slope-log area plot. However, wide  
211 variation in  $k_s$  (regression intercept) can be the corollary of a small variation in  $\theta$  (regression  
212 slope). So, relying on the assumption of a restricted range of the concavity index in a steady  
213 state ( $0.4 \leq \theta \leq 0.6$ ) (Kirby and Whipple, 2001; Kirby and Whipple, 2012; Snyder et al.,  
214 2000; Wobus et al., 2003; Wobus et al., 2006), the normalized steepness index ( $k_{sn}$ ) can be  
215 determined by evaluating slope-area regression using a reference concavity ( $\theta_{ref} = 0.45$ ) in  
216 Eq. (2).

$$217 \quad S = k_{sn} A^{-\theta_{ref}} \quad (2)$$

218 Here, the variation in drainage area can be surmounted and effective comparison between  
219 streams profiles can be achieved, regardless of their catchment areas. In equilibrium  
220 landscapes, similar concavities for multiple segments of a stream profile can be recognised,  
221 but not similar steepness. Uplift results in steepened rivers, and accordingly the steepness  
222 index will vary (Dietrich et al., 2003; Snyder et al., 2000). Thus,  $k_{sn}$  can be used as a suitable  
223 metric in tectonic geomorphology studies (Kirby and Whipple, 2001; Wobus et al., 2006).

224 The SRTM 30 dataset (30 m pixel size) was used for the purpose of drainage network  
225 extraction, using MATLAB-based TecDEM 2.2 software (Shahzad and Gloaguen, 2011). The  
226 D8 algorithm (Jones, 2002) was applied to calculate flow directions.

227 The first step in deriving  $k_{sn}$  values is river profile generation. For this process, a minimum  
228 threshold of  $10^5 \text{ m}^2$  contributing area was used to ensure fluvial dominated channel flow  
229 (Kirby and Whipple, 2001; Montgomery and Foufoula-Georgiou, 1994; Wobus et al., 2006).  
230 Using Stream Profiler software, the  $k_{sn}$  value was calculated for the whole Zagros using a  
231 reference concavity of  $\theta_{ref} = 0.45$  (Wobus et al., 2006) to overcome lithological effects on the  
232 concavity index, and consequently the steepness index. Also we used TopoToolbox 2  
233 MATLAB-based software (Schwanghart and Scherler, 2014) to calculate the  $k_{sn}$  of all river  
234 segments across the Zagros which have length more than 1 km. Results were compared with

235 lithologies represented on geological maps, to determine whether HI values are affected by  
236 active tectonic or lithological changes.

237 SRTM data have inherent errors (Boulton and Stokes, 2018) which result in voids that affect  
238 the flow-routing algorithm. Therefore, to test the method of river profile extraction, the  
239 QaraChwalan River profile was extracted manually from the SRTM 30 m data using Global  
240 Mapper GIS, and compared with the automatic extracted profile (supplementary Fig. 2). No  
241 difference was found between the two profiles, which indicates the reliability of the automatic  
242 drainage network extraction technique.

#### 243 **2.4. Hypsometric Index (HI)**

244 The idea of hypsometry was first used to express the forms of drainage basins (catchments)  
245 and their slopes (Langbein, 1947). Strahler (1952) introduced the idea of the hypsometric  
246 index, or integral (HI).

247 For a given drainage basin, HI refers to the amount of residual terrain above the lowest  
248 horizontal plane of a basin and it can be used as a proxy for the erosional stage and landform  
249 development (Strahler, 1952; Schumm, 1956). High HI values (close to 1) mean that uplift is  
250 greater than erosion and the land surface is in a youthful stage, while low HI values (close to  
251 0), erosion is greater than uplift and the land surface is in a mature stage. This dimensionless  
252 form enables the comparison between different basins regardless of their areas.

253 HI is a powerful tool to investigate the relative tectonism of an area, by characterizing the  
254 topographic dissection of a basin (Keller and Pinter, 2002). Due to the development of Digital  
255 Elevation Models (DEMs), HI can be calculated using Eq. (3) (Pike and Wilson, 1971; Keller  
256 and Pinter, 2002).

$$257 \quad HI = \frac{H_{mean} - H_{min}}{H_{max} - H_{min}} \quad (3)$$

258 Where  $H_{max}$ ,  $H_{min}$ , and  $H_{mean}$  are the maximum, minimum, and mean elevations respectively.  
259 We adopt the approach of Gao et al. (2016), who measured HI for drainage basins of a  
260 particular stream order to map out regional variations in the east of the Tibetan Plateau. The  
261 rationale is that drainage basins are naturally-defined areas that reflect both tectonics and  
262 lithology, and so align with changes in one or both of these parameters (e.g. slip and uplift on  
263 active faults).

264 The parameters of Eq. (3) were obtained directly from DEM data and HI was calculated using  
265 TecDEM 2.2 MATLAB-based and standard ArcGIS 10.3.1 software. The HI data were  
266 converted into raster mode using the polygon to raster function within the ArcGIS 10.3.1 to  
267 extract swath profiles for the HI data across different regions in the Zagros.

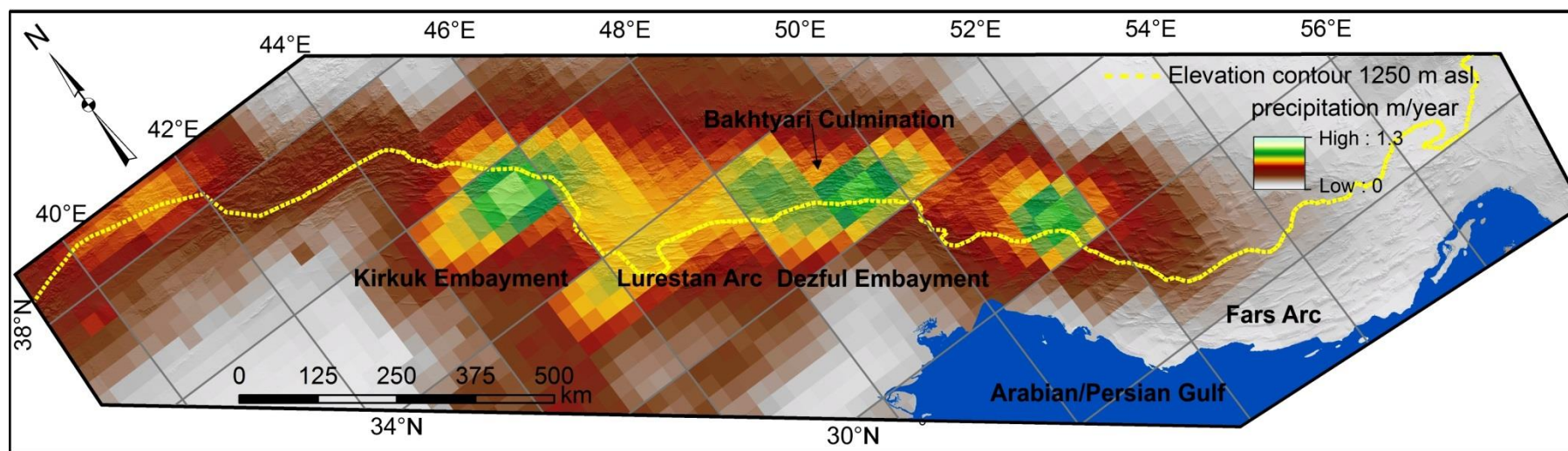
268 HI values for 4<sup>th</sup> order (supplementary Fig. 3a) 5<sup>th</sup> order (supplementary Fig. 3b) and 6<sup>th</sup> order  
269 river basins (supplementary Fig. 3c) have been tested for a comparative analysis of HI values  
270 at different scales of drainage (supplementary Fig. 3a, b and c). The distribution of HI classes  
271 across the Zagros is similar for all orders of river basins, but the large area basins (i.e. 6<sup>th</sup>  
272 order) lack enough resolution to distinguish changes in HI values and hence potential changes  
273 in tectonic style. Thus, the use of the third order river basin is preferred as it gives more  
274 detailed results about landscape response to tectonics. Using second or first order basins  
275 introduced problems because of the extra processing time required, and artefacts introduced  
276 by the resolution of the DEM data and the ability of the software to define drainage basins  
277 accurately.

### 278 **3. Results**

#### 279 **3.1. Climate**

280 The TRMM 3B43 data show high variability in precipitation across different regions of the  
281 Zagros (Fig. 2), taking average annual values from the dataset. The maximum precipitation (~  
282 0.35 m/year) occurs in the Bakhtyari Culmination, parts of Lurestan and the northeast of the  
283 Kirkuk Embayment. The minimum precipitation (0.05 m/year) occurs in the central and  
284 eastern Fars regions, the interior of the Turkish-Iranian Plateau and in the foreland. In the  
285 Discussion we look at the geomorphic and tectonic data in the light of this climatic variation.

286



287

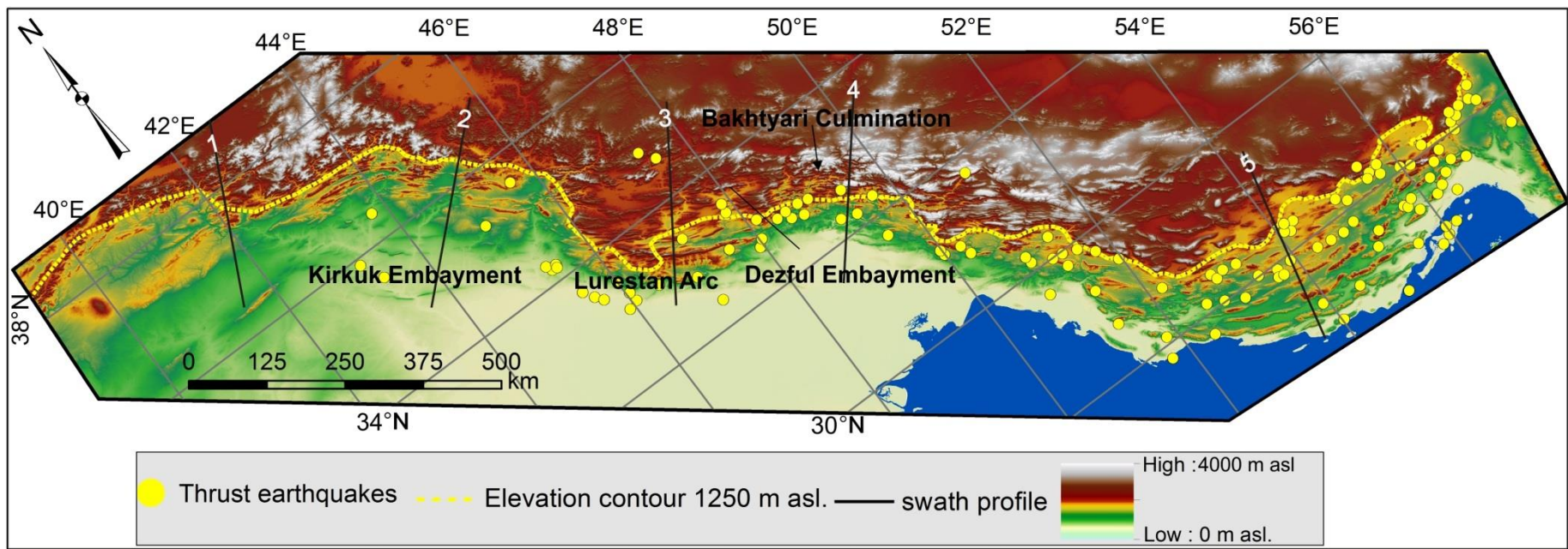
288 Fig. 2. SRTM 30 m shaded relief map of the Zagros, overlain by mean annual precipitation from the TRMM satellite

289 (<https://mirador.gsfc.nasa.gov/>) for the period 1998-2016. Note the difference in precipitation between the Fars and Dezful/Bakhtyari regions.

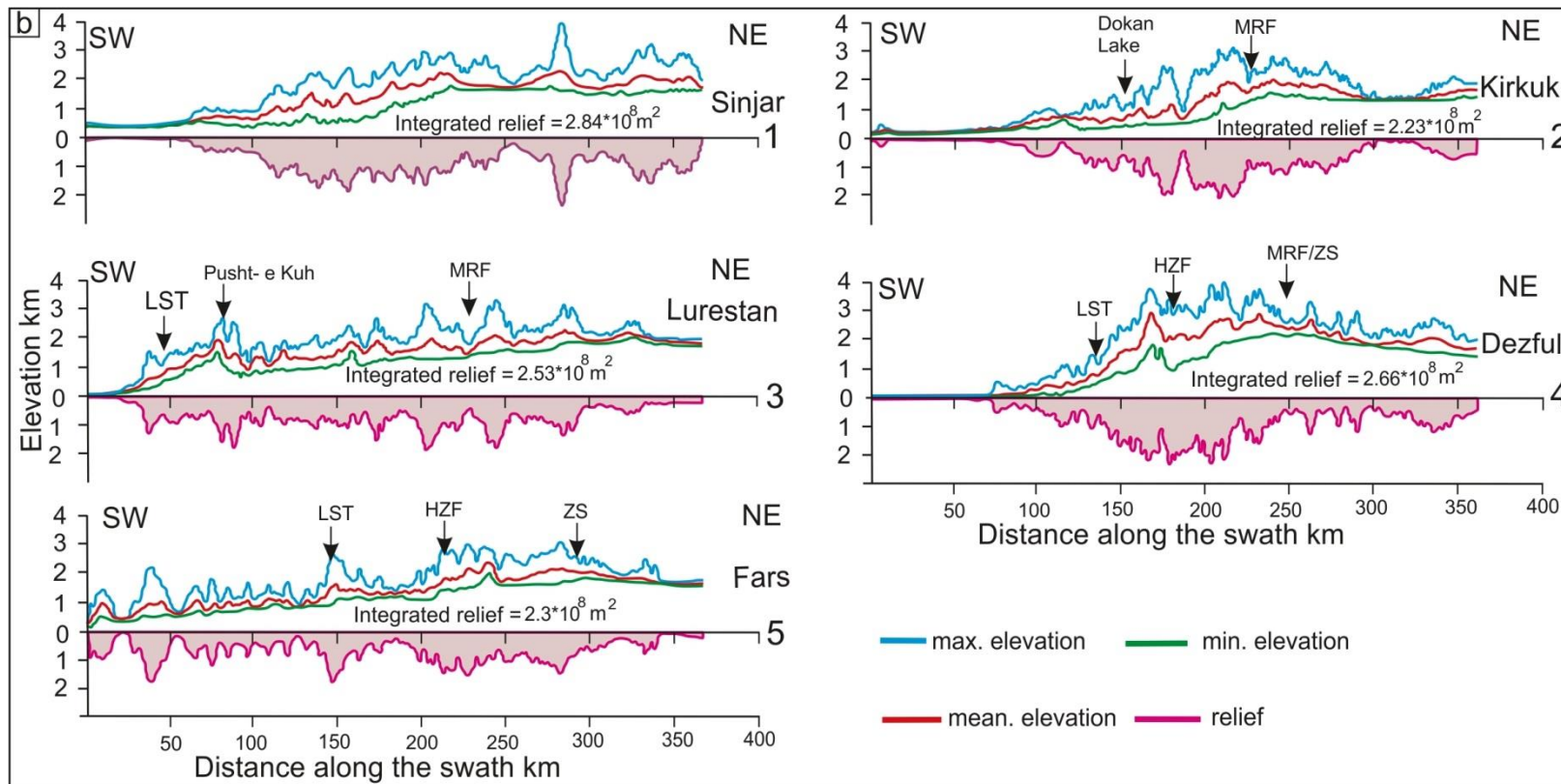
290

291 **3.2. Topographic swath profile analysis**

292 Five swath profiles across the Zagros are shown in Fig. 3 as representative of the 25 analysed.  
293 These profiles show variations in topography across different regions of the range. The  
294 difference in elevation (relief) varies from  $\sim < 50$  m within the Dezful Embayment to  $> 2500$  m  
295 in the Bakhtyari Culmination. Some profiles exhibit a gradual decline in elevation towards the  
296 foreland such as the Sinjar and Kirkuk profiles. Other profiles show a sharp drop towards the  
297 foreland, such as the Lurestan and Dezful examples. There is an increase in elevation and  
298 gradient towards the hinterland at or near the limit of seismogenic thrusting at 1250 m  
299 elevation (Allen et al., 2013) in both the Lurestan and Dezful sections. In contrast, there are  
300 very gentle changes in elevation across the Fars region, even when passing through the thrust  
301 seismicity cut-off at  $\sim 1250$  m elevation, and across the High Zagros Fault. The difference  
302 between the maximum and the minimum elevations within the swaths (relief) shows where  
303 river networks dissect the landscapes. We integrate the relief of swath profiles (Fig. 3b). The  
304 cumulative difference between the maximum and minimum elevations (shaded areas in Fig.  
305 3b) shows a difference of  $\sim 25\%$  between the five profiles.



306



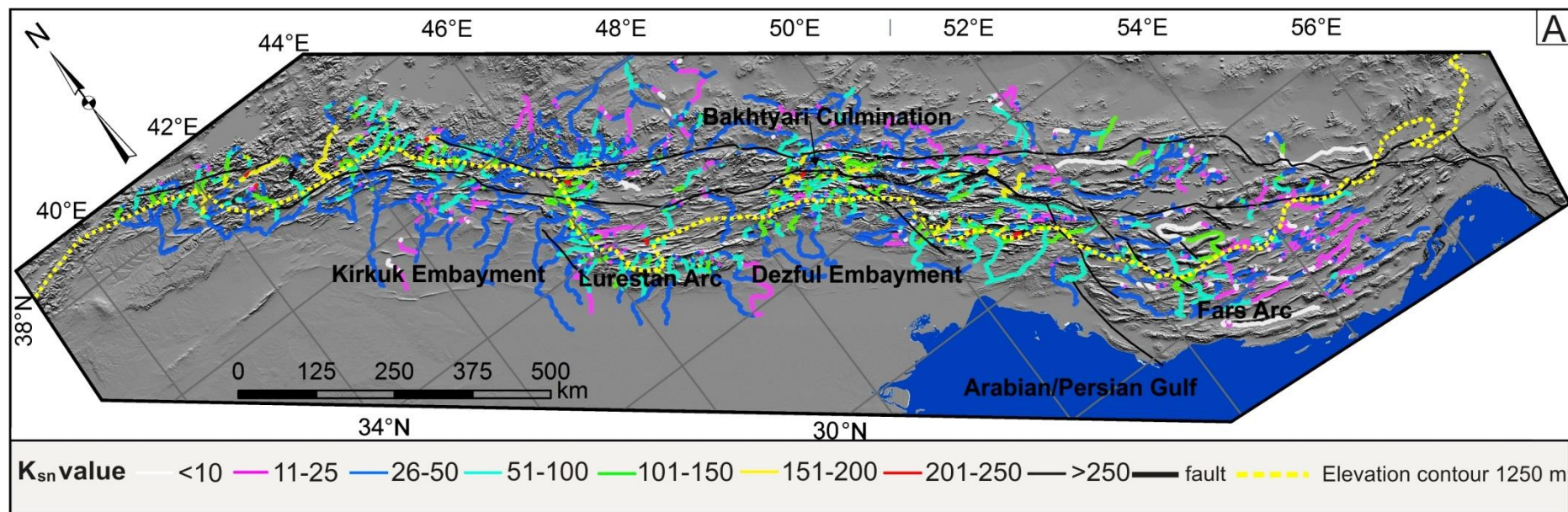
307

308 Fig. 3. SRTM 30 m topography of the Zagros fold-and-thrust belt. (a) Locations for topographic swath profiles. (b) Mean, Maximum and  
 309 minimum elevation along the swath profiles. Integrated relief graphs show a limited relief difference in the order of ~25% between representative  
 310 swath profiles. LST = Limit of seismogenic thrusting; HZF = High Zagros Fault; MRF = Main Recent Fault; ZS = Zagros Suture.

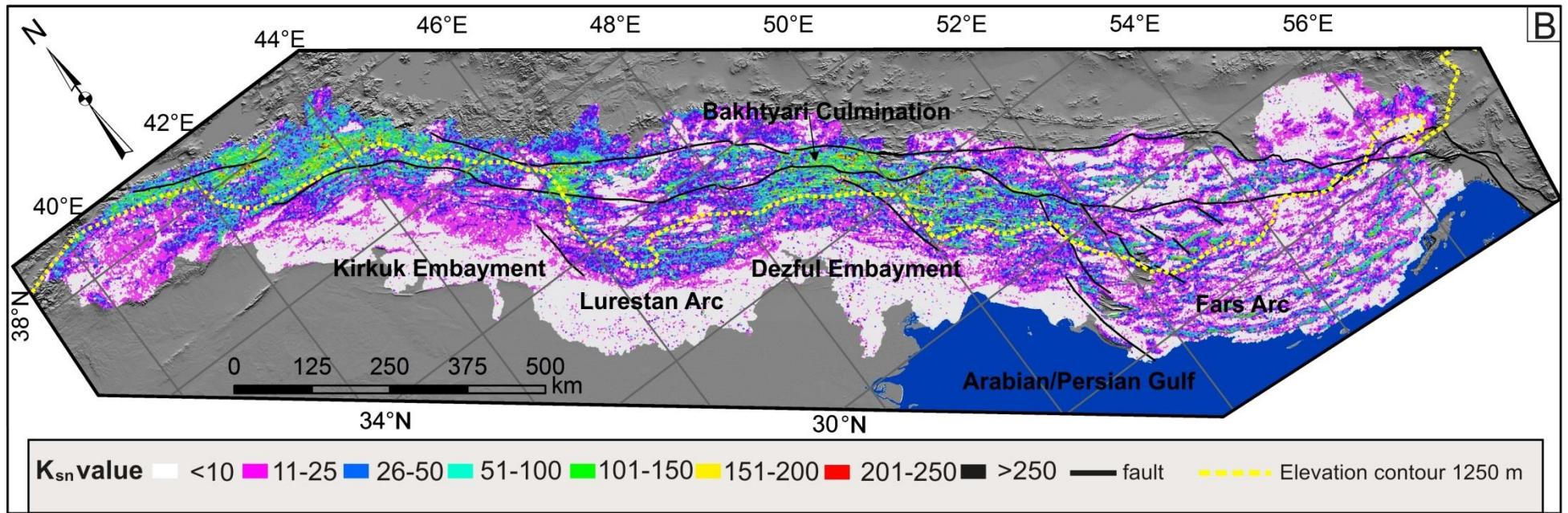
311 **3.3. Normalized river-channel steepness ( $k_{sn}$ )**

312 Longitudinal profiles (supplementary figure 4) were generated for all river segments with a  
313 length of more than 1 km (Fig. 4a and b). Reaches of  $k_{sn} < 50 \text{ m}^{0.9}$  are distributed across the  
314 Iranian plateau, the foreland, intermontane rivers and the Fars region (Fig. 4). Ranges of  $50 \leq$   
315  $k_{sn} \leq 100 \text{ m}^{0.9}$  occur in the high relief areas of the Bakhtyari Culmination, Sirwan River basin,  
316 and in terrain at close the 1250 m elevation contour in the NW Zagros, near the Iraq-Turkey  
317 border (Fig. 4). A similar distribution occurs across the high relief areas when considering the  
318 range of  $100 \leq k_{sn} \leq 150 \text{ m}^{0.9}$  (Fig. 4). Values of  $k_{sn} \geq 150 \text{ m}^{0.9}$  occur only for a few river  
319 segments in the high relief areas of the Bakhtyari and the NW Zagros of Iraq and Turkey  
320 (Fig.4). Generally, the Fars region exhibits relatively low  $k_{sn}$  values compared with other  
321 areas of the Zagros (Fig. 4).

322



323



324

325 Fig.4. Distribution of  $k_{sn}$  values for Zagros river segments. (a)  $k_{sn}$  values using MATLAB-Based stream profiler; note the low values in the Fars  
 326 region. (b)  $k_{sn}$  values extracted using TopoToolbox software. Note the high values in the Bakhtyari Culmination and the northeast of the Kirkuk  
 327 Embayment.

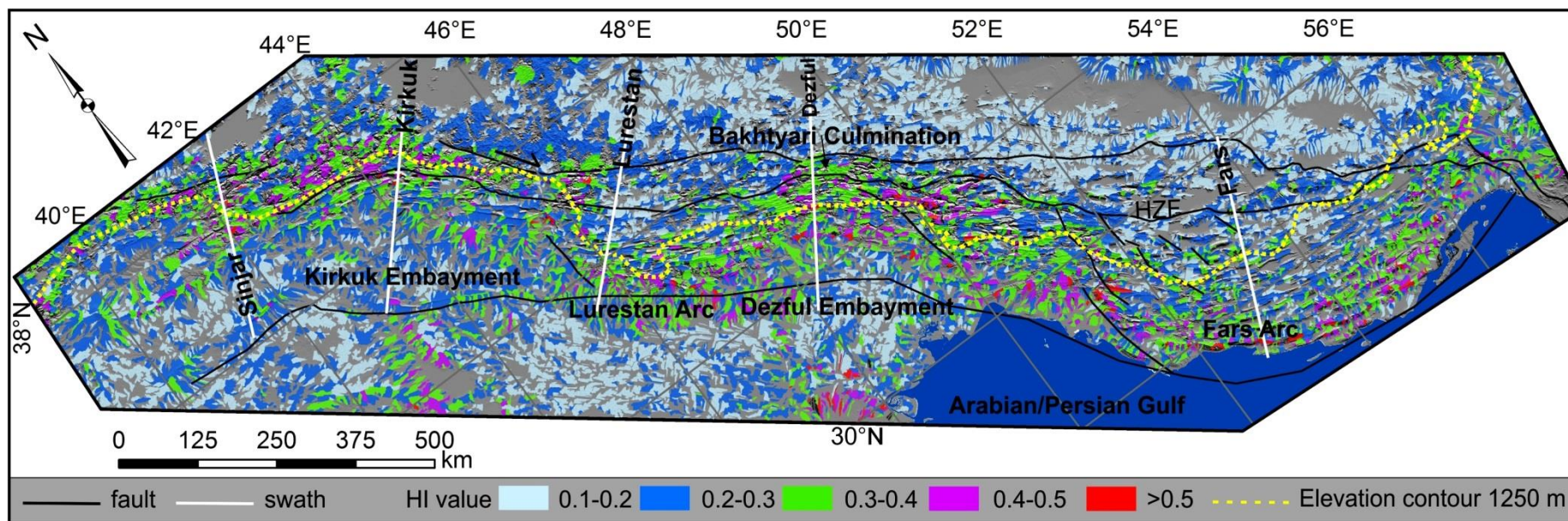
### 328 **3.4. Hypsometric Index (HI)**

329 Results from 17380 third order river basins across the Zagros reflect two major groups of  
330 relative low HI values ( $HI < 0.3$ ) (Fig. 5). The first group of relative low HI values represents  
331 the Turkish-Iranian Plateau where topographic gradients are very low (Allen et al., 2013). The  
332 second group of relative low HI region occurs across the foreland and Mesopotamian plain.  
333 Intermediate and relatively high HI values ( $> 0.3$ ) occur across the mountainous areas of the  
334 Zagros which are characterized by high relief and gradient (Fig. 6). Highest values occur  
335 northeast of the Kirkuk Embayment, in the Bakhtyari Culmination, and close to the coast in  
336 the Fars region (Fig. 5).

337 Along much of the Zagros there is a coincidence between the transition limit from HI values  
338 of  $< 0.3$  to  $> 0.3$  upper elevation limit of seismogenic thrusting (Fig. 5). This pattern is seen  
339 northeast of the Kirkuk Embayment, along the Lurestan/Pusht-e Kuh Arc and in the region of  
340 the Kazerun Fault (western Fars). Different patterns occur in the Bakhtyari Culmination and  
341 in the southeast of the Zagros (Fars region). In the Bakhtyari Culmination relatively high HI  
342 values persist northeast of (above) the 1250 m elevation contour and the limit of seismogenic  
343 thrusting. In the Fars region, seismogenic thrusting continues north of the transition from high  
344 to low HI values (taken as  $HI = 0.3$ ).

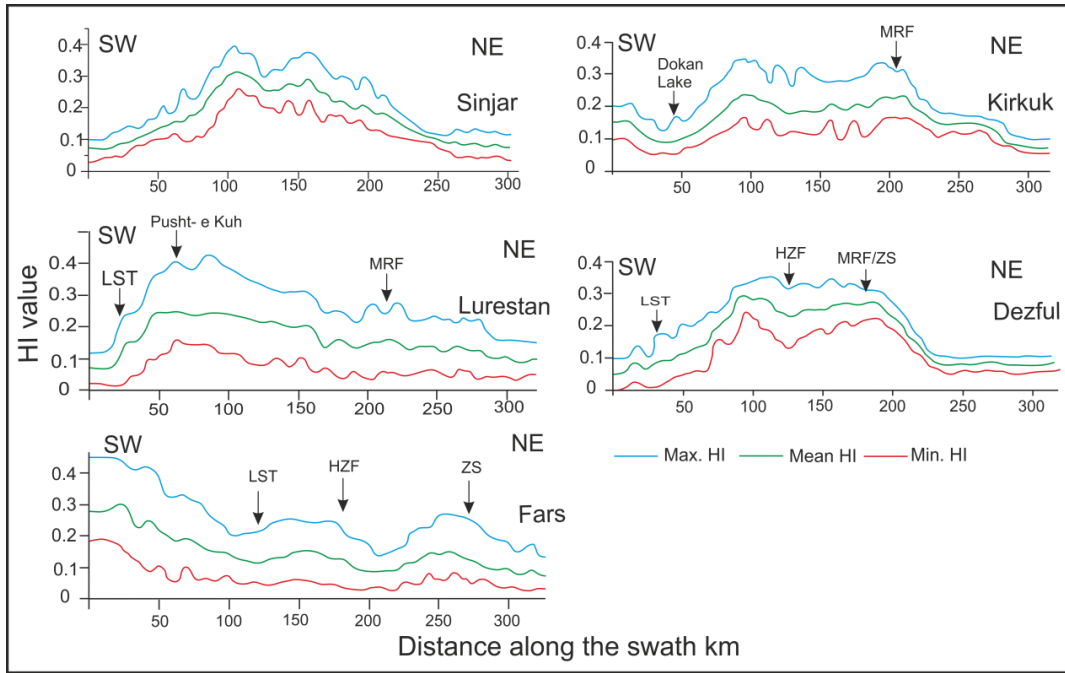
345 Swath profiles from raster data of the HI value across the Zagros (Fig. 6) show the HI value  
346 increasing in areas of high relief but not within high elevation regions. Differences in  
347 lithology have been examined to assess whether lithology is a significant control on HI value:  
348 Figure 7 shows both HI values and lithologies for the Bakhtyari Culmination; there is no clear  
349 correlation between them.

350



351

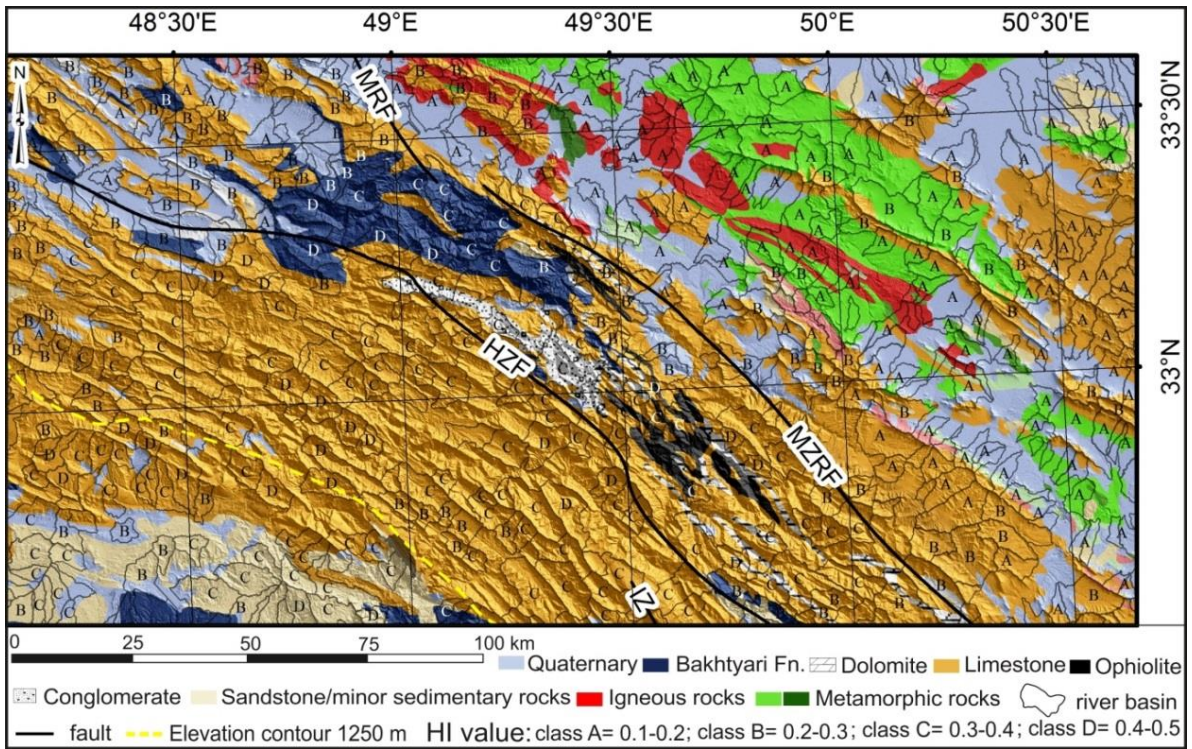
352 Fig. 5. HI values for 3<sup>rd</sup> order drainage basins across the Zagros. There is a broad region of relative high HI (>0.3; green-amethyst colours) along  
353 the Zagros, between the Iranian Plateau and the foreland. Specific regions show variations to this broad trend. In the Bakhtyari Culmination, the  
354 high/low HI transition lies at higher elevations than the thrust seismicity cut-off (~1250 m elevation contour), while in the Fars region the  
355 high/low HI transition takes place at lower elevations than this cut-off.



356

357 Fig.6. Swath profiles extracted from HI raster data show the variation in HI across the Zagros  
 358 range along the swaths in Fig. 5. The width of swaths is 25 km on either side of the swath  
 359 centre. LST = Limit of seismogenic thrusting; ZS = Zagros Suture; HZF = High Zagros Fault;  
 360 MRF = Main Recent Fault. The Fars region has high HI values southwest of the LST, in the  
 361 opposite sense to the Dezful region.

362



363

364 Fig. 7. HI values in the Bakhtyari Culmination plotted over the geological map (geology from  
365 sources in Fig. 1b), which shows similar HI values across different lithologies, and different  
366 HI values across the same lithology.

## 367 **4. Discussion**

### 368 **4.1. Swath profiles**

369 The Sinjar, Kirkuk and Fars sections show steady increases in elevation toward the hinterland  
370 for the first ~200 km of the swath profiles (Fig. 3), which is well-established by previous  
371 work (see McQuarrie, 2004; Mouthereau et al., 2012; Allen et al., 2013 and references  
372 therein). Integrating the relief along each profile (Fig. 3) shows the values for each profile are  
373 within ~25% of each other, at  $2.2 - 2.8 \times 10^8 \text{ m}^2$ . Given that this is a new approach to  
374 analyzing the geomorphology of active fold-and-thrust belts, it is not possible to make  
375 detailed comparisons with other ranges. However, we suggest that a ~25% variation is not  
376 large, considering the variation in structure and climate in different parts of the Zagros. This  
377 in turn suggests that the integrated relief of the mountain range may be less controlled by the  
378 parameters which vary along the Zagros, such as the width of the seismogenic belt, or  
379 maximum topographic gradient, and more by parameters which are similar across strike, such  
380 as strain rate (Masson et al., 2005), overall shortening (McQuarrie, 2004; Vergés et al., 2011;  
381 Allen et al., 2013), or the elevation difference between the hinterland plateau and the  
382 undeformed foreland.

### 383 **4.2. Normalized river-channel steepness ( $k_{sn}$ )**

384 Bearing in mind that surface uplift is extremely unlikely to be uniform across the entire  
385 Zagros, with implications for the applicability of a uniform approach to analyzing  $k_{sn}$  (Snyder  
386 et al., 2000), there are broad differences in  $k_{sn}$  values as follows. There is a general pattern  
387 that higher  $k_{sn}$  values occur where the rivers cross the 1250 m contour (Fig. 4), and so from  
388 the interior, relatively aseismic region into the thrust-seismogenic part of the Zagros, but this  
389 is a broad distinction, without a sharp change.  $k_{sn}$  values are lower in the Fars region than  
390 elsewhere in the Zagros. Kirby and Whipple (2012) noted the correlation between the linear  
391 physiographic transition of Lesser/Greater Himalaya and the northward increase in  $k_{sn}$  values.  
392 The zone of high  $k_{sn}$  values is on the hanging wall of the Himalayan Main Central Thrust  
393 (MCT), interpreted as relating to the active uplift in the vicinity of this fault. The  
394 Longmenshan in SE Tibet is another example of a sharp boundary between high and low  $k_{sn}$   
395 values, in the region of the active Yingxiu-Beichuan and Pengguan faults (Gao et al., 2016).

396 Such sharp distinctions have not been found in the  $k_{sn}$  distribution of the Zagros, perhaps due  
397 to the tectonic difference between the multiple, segmented, blind thrusts of the Zagros, and  
398 the laterally continuous and large scale thrusts of the Himalaya (i.e. the MCT) and SE Tibet.

399 Rivers in the Fars region commonly divert around the tips of anticlines or cross relay zones  
400 between them. This is because of low discharge of rivers including the internally drained  
401 basins in the region. The relatively dry climate has led to limited and ephemeral discharge of  
402 rivers which is not enough to overcome the growth of anticlines. Therefore the Fars region  
403 rivers have low  $k_{sn}$  values (Fig. 4) and commonly divert around anticlines (Ramsey *et al.*,  
404 2008). Although there are many anticlines and active seismicity in the Fars region, the dry  
405 climate has an important effect in the formation of axial rivers (Ramsey *et al.*, 2008).  
406 Transverse rivers commonly occur in the Dezful/Bakhtyari region as a result of relatively  
407 high precipitation and intense thrusting in the Bakhtyari Culmination, which enable rivers to  
408 incise as they cross numerous anticlines.

#### 409 **4.3. Hypsometric Index (HI)**

410 In the Bakhtyari Culmination (Fig. 7) we examine changes in bedrock lithologies and their  
411 effects on the HI value. The Culmination consists mainly of limestones, limestones alternating  
412 with marls and conglomerates, patches of ophiolitic lithologies (e.g. serpentinite, basalt), and  
413 sandstones and conglomerates of the Bakhtyari Formation. To the northeast of the  
414 Culmination there is a series of igneous and metamorphic rocks. For the same lithology there  
415 are significant differences in the HI value. In contrast, there are areas where different  
416 lithologies, such as the ophiolitic assemblages and limestones, show similar HI values (0.3-  
417 0.4) (Fig. 7). This result implies that differences in lithology have limited effects on the HI  
418 value.

419 Figure 2 shows the climatic variation within and across the Zagros, with a seven-fold  
420 difference between annual precipitation in the wettest areas (Dezful/Bakhtyari Culmination)  
421 and the driest areas (parts of Fars). The relatively wet climate in the Dezful/Bakhtyari regions  
422 (Fig. 2) enables the river system to erode the landscape in an area where deformation takes  
423 place predominantly in a narrow zone of high strain (Allen *et al.*, 2013) and steep slopes: the  
424 Bakhtyari Culmination. The high HI region continues to the northeast of the seismogenic limit  
425 of thrusting (Fig. 5). From the tectonic perspective, this region has become part of the  
426 Turkish-Iranian Plateau, in that it is not experiencing active (seismogenic) shortening; from a

427 geomorphic perspective, it has not yet become a relatively low relief plateau, because of the  
428 relief created and maintained by the drainage network (Figs. 5 and 6).

429 In the Fars region, the exposed lithology is mainly limestone, which resists erosion on the  
430 flanks and crests of anticlines (Fig. 1). The relatively dry climate in Fars (Fig. 2), combined  
431 with low regional gradients and sinuous rivers, reduces stream power, and thus erosion rates.  
432 Consequently, the low HI zone occurs south of the limit of seismogenic thrusting (Fig. 5).  
433 This part of the Fars region behaves in the opposite sense to the Dezful/Bakhtyari region, in  
434 that it still experiences thrust seismicity, even in a low relief area that resembles the  
435 essentially aseismic plateau interior further north (Fig. 8). We attribute the difference in the  
436 location of the low/high HI transition to differences in the basement of the Dezful/Bakhtyari  
437 and Fars regions. Deformation is focused in the Bakhtyari Culmination because the adjacent  
438 Dezful Embayment resists deformation, attributed by Allen and Talebian (2011) to the  
439 different pre-collisional histories of the Dezful Embayment and adjacent areas. There is no  
440 difference within the Fars region (Allen et al., 2013; Talebian and Jackson, 2004). These  
441 tectonic differences have a climatic positive feedback result in the relatively wet climate in  
442 the Dezful/Bakhtyari, where there is a higher topographic barrier, while in contrast, a  
443 relatively dry climate and low relief occur in the Fars region (Figs. 1, 2 and 5).

444 Regional analysis of HI values on a drainage basin scale does not show sharp changes across  
445 individual structures, which would be expected if active deformation was controlled by a  
446 small number of major thrusts in the Zagros. This pattern contrasts with the east of the  
447 Tibetan Plateau (Longmenshan), where such abrupt jumps in HI have been observed (Gao et  
448 al., 2016).

449 In the Zagros study area, HI is a more effective tool than  $k_{sn}$  analysis, for highlighting  
450 geomorphic variations that relate to the active tectonics and climate. We do not make this as a  
451 universal claim, but it will be interesting to apply HI analysis in the form used by Gao et al  
452 (2016) and in this paper, to other active fold-and-thrust belts in the world.

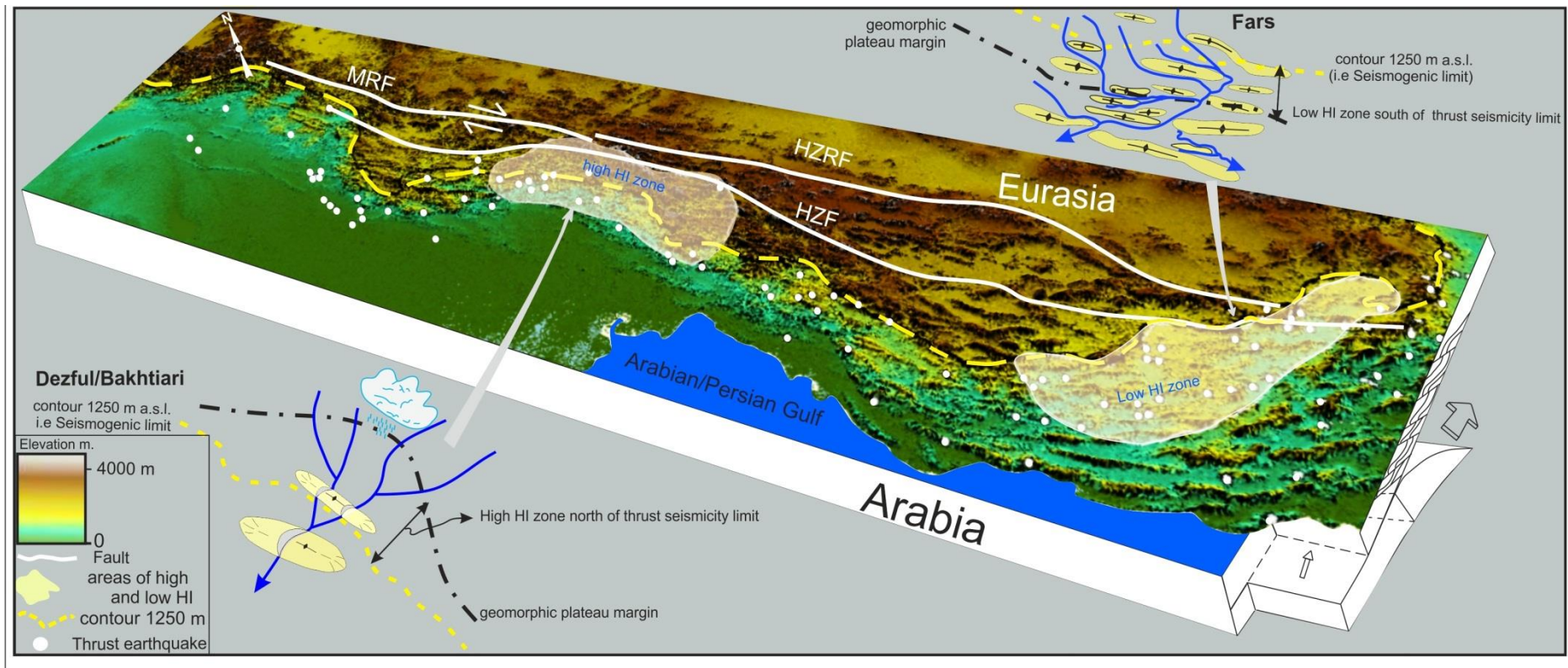
## 453 **5. Conclusions**

454 In this paper we show that the geomorphic index HI provides insights into the landscape  
455 response to tectonics and climate in the Zagros (Fig. 5), and it is more effective in this regard  
456 than the more commonly used  $k_{sn}$  analysis (Fig. 4). Differences in geomorphic indices across  
457 two specific areas in the Zagros can be explained by the different climate of the two areas:

458 wetter conditions and vigorous drainage systems in the Dezful/Bakhtyari region retard plateau  
459 growth; drier climate leads to low stream power of rivers in the Fars region and promotes  
460 plateau growth (Fig. 8). The cut-off in thrust seismicity, proxied by the 1250 m elevation  
461 contour, provides a simple tectonic boundary marker for comparison (Nissen et al., 2011).  
462 Orographic precipitation may itself have a tectonic control; regional basement strength  
463 variations are another plausible cause (Allen and Talebian, 2011). Strong basement in the  
464 Dezful Embayment keeps the amount of strain low in this region, but produces intense  
465 thrusting and steep relief in the Bakhtyari Culmination to its northeast, so that the overall  
466 strain across this part of the Zagros is similar to adjacent regions (Allen and Talebian, 2011).  
467 It is possible that the Kirkuk Embayment has a similar origin to the Dezful Embayment, with  
468 the same consequence, that high strain is concentrated in the imbricate zone to its northeast  
469 where high  $k_{sn}$ , HI and high relief occur.

470 We conclude that there is a positive feedback of tectonics and climate, which leads to the  
471 wetter climate in the Bakhtyari Culmination, and causes rivers to cut efficiently through  
472 landscapes. Youthful, high relief landscapes are the result, in contrast with the drier climate of  
473 the Fars region: the Fars climate promotes subdued landscapes and plateau-like  
474 geomorphologies in an area that is actively shortening by seismogenic thrusting.

475 Integrated relief along five topographic swath profiles is similar to within ~25% (Fig. 3).  
476 These profiles are different to each other in terms of the distribution of elevation and climate.  
477 We argue that the degree of relative similarity between the integrated relief is related to one or  
478 more of the parameters that are similar between different regions, such as such as strain rate,  
479 overall shortening, or the elevation difference between the hinterland plateau and the  
480 undeformed foreland.



482

483 Fig. 8. Model showing how the Zagros topography responds to tectonism in term of changes in HI value. Relative high and relative low HI  
 484 regions relate to the cut-off in thrust seismicity (proxied by the 1250 m elevation contour). The geomorphic plateau margin is retarded to the  
 485 northeast in the Dezful/Bakhtyari region, and advances southwest in the Fars region.

486 **Acknowledgements**

487 We thank the Ministry of Higher Education and Scientific Research in Iraq for their support  
488 of the first author's project. We thank Chris Saville for useful discussion of geomorphic  
489 indices and Sarah Boulton for her help with stream profile analysis. The first author would  
490 like to thanks the Institution of Geological Survey of Iraq (GEOSURV) for providing  
491 geological maps included in this paper. Christoph Grützner and David Fernández-Blanco  
492 provided constructive reviews. We are grateful to Christoph von Hagke and Olivier Lacombe  
493 for handling the editorial process.

494 **References**

- 495 Afaghi, A, Salek, M. M., 1975a. Geological map of Iran, sheet No., 5 North-west Iran,  
496 National Iranian Oil Company, Tehran, Iran, scale 1:1,000,000.
- 497 Afaghi, A, Salek, M. M., 1975b. Geological map of Iran, sheet No., 4 South-West Iran,  
498 National Iranian Oil Company, Tehran, Iran, scale 1:1,000,000.
- 499 Afaghi, A, Salek, M. M., 1977a. Geological map of Iran, sheet No., 2 North-Central Iran,  
500 National Iranian Oil Company, Tehran, Iran, scale 1:1,000,000.
- 501 Afaghi, A, Salek, M. M., 1977b. Geological map of Iran, sheet No., 3 North-East Iran,  
502 National Iranian Oil Company, Tehran, Iran, scale 1:1,000,000.
- 503 Afaghi, A, Salek, M. M., 1977c. Geological map of Iran, sheet No., 6 South-East Iran,  
504 National Iranian Oil Company, Tehran, Iran, scale 1:1,000,000.
- 505 Afaghi, A, Salek, M. M., Moazami, J., 1978. Geological map of Iran, sheet No., 1 North-west  
506 Iran, National Iranian Oil Company, Tehran, Iran, scale 1:1,000,000.
- 507 Alavi, M., 2007. Structures of the Zagros fold-thrust belt in Iran. *American Journal of Science*  
508 307, 1064–1095.
- 509 Allen, M. B., Armstrong, H. A., 2008. Arabia-Eurasia collision and the forcing of mid-  
510 Cenozoic global cooling. *Palaeogeography, Palaeoclimatology, Palaeoecology*. 265, 52–  
511 58.
- 512 Allen, M. B., Talebian, M., 2011. Structural variation along the Zagros and the nature of the  
513 Dezful Embayment. *Geological Magazine* 148, 911-924.  
514 doi:10.1017/S0016756811000318.
- 515 Allen, M. B., Saville, C., Blanc, E. J.-P., Talebian, M., Nissen, E., 2013. Orogenic plateau  
516 growth: Expansion of the Turkish-Iranian Plateau across the Zagros fold-and-thrust belt,  
517 *Tectonics* 32, 171–190, doi:10.1002/tect.20025.

- 518 Ameen, M. S., 1992. Effect of basement tectonics on hydrocarbon generation, migration, and  
519 accumulation in Northern Iraq. *American Association of Petroleum Geologists Bulletin*  
520 76, 356–370.
- 521 Andreani, L., Stanek, P. K., Gloaguen, R., Krentz, Ottomar, Dominquez-Gonzalez, L., 2014.  
522 DEM-Based Analysis of interactions between tectonics and landscapes in the Or  
523 Mountain and Eger Rift (East Germany and NW Czech Republic). *Remote Sensing* 6,  
524 7971–8001.
- 525 Bahrami, S., 2013. Analyzing the drainage system anomaly of zagros basins: Implications for  
526 active tectonics. *Tectonophysics* 608, 914–928.
- 527 Berberian, M., 1995. Master “blind” thrust faults hidden under the Zagros folds: active  
528 basement tectonics and surface morphotectonics. *Tectonophysics* 241, 193–224.
- 529 Blanc, E. J.-P., Allen, M. B., Inger, S., Hassani, H., 2003. Structural styles in the Zagros  
530 Simple Folded Zone, Iran. *Journal of the Geological Society* 160, 40–412.
- 531 Boroujerdy, P., Nasrollahi, N., Hsu, K., Sorooshian, S., 2013. Evaluation of satellite-based  
532 precipitation estimation over Iran. *Journal of Arid Environments* 97, 205–219.
- 533 Boulton, S.J., Whittaker, A.C., 2009. Quantifying the slip rates, spatial distribution and  
534 evolution of active normal faults from geomorphic analysis: Field examples from an  
535 oblique-extensional graben, southern Turkey. *Geomorphology* 104, 299–316.
- 536 Boulton, S.J., Stokes, M., 2018. Which DEM is best for analyzing fluvial landscape  
537 development in mountainous terrains? *Geomorphology* 310, 168-187.
- 538 Bowman, D., Shachnovich-Firtel, Y., Devora, S., 2007. Stream channel convexity induced by  
539 continuous base level lowering, the Dead Sea, Israel. *Geomorphology* 92, 60–75.  
540 doi:10.1016/j.geomorph.2007.02.009.
- 541 Bretis, B., Bartl, N., Grasemann, B., 2011. Lateral fold growth and linkage in the Zagros fold  
542 and thrust belt (Kurdistan, NE Iraq). *Basin Research* 23, 615–630.
- 543 Burberry, C.M., Cosgrove, J.W. and Liu, J.G., 2008. Spatial arrangement of fold types in the  
544 Zagros Simply Folded Belt, Iran, indicated by landform morphology and drainage  
545 pattern characteristics. *Journal of Maps* 4, 417-430.
- 546 Burberry, C. M., Cosgrove, J. W. Liu, J.-G., 2010. A study of fold characteristics and  
547 deformation style using the evolution of the land surface: Zagros Simply Folded Belt,  
548 Iran. *Geological Society, London, Special Publications* 330,139-154.
- 549 Burberry, C. M. 2015. The effect of basement faults reactivation on the Triassic-Recent

550 geology of Kurdistan , North Iraq. *Journal of Petroleum Geology* 38, 37–58.

551 Casciello, E., Vergés, J., Saura, E., Casini, G., Fernandez, N., Blanc, E., Homke, S., Hunt,  
552 D.W., 2009. Fold patterns and multilayer rheology of the Lurestan Province, Zagros  
553 Simply Folded Belt (Iran). *Journal of the Geological Society* 166, 947–959.

554 Dietrich, W.E., Bellugi, D.G., Heimsath, A.M., Roering, J.J., Sklar, L.S., Stock, J.D., 2003.  
555 Geomorphic Transport Laws for Predicting Landscape Form and Dynamics. *Geophys.*  
556 *Monogr.* 135, 1–30. doi:10.1029/135GM09

557 Fakhari, M.D., Axen, G.J., Horton, B.K., Hassanzadeh, J., Amini, A., 2008. Revised age of  
558 proximal deposits in the Zagros foreland basin and implication for Cenozoic evolution of  
559 the High Zagros. *Tectonophysics* 451, 170–185.

560 Flint, J.J., 1974. Stream gradient as a function of order, magnitude, and discharge. *Water*  
561 *Resources Research* 10, 969–973. doi:10.1029/WR010i005p00969.

562 Gao, M., Zeilinger, G., Xu, X., Tan, X., Wang, Q., Hao, M., 2016. Active tectonics evaluation  
563 from geomorphic indices for the central and the southern Longmenshan range on the  
564 Eastern Tibetan Plateau, China. *Tectonics*, 35, 1812–1826, doi:10.1002/2015TC004080.

565 Ghasemi, A., Talbot, C., 2006. A new tectonic scenario for the Sanandaj-Sirjan Zone (Iran).  
566 *Journal of Asian Earth Sciences* 26, 683–693.

567 Goldrick, G., Bishop, P., 2007. Regional analysis of bedrock stream long profiles: evaluation  
568 of Hack’s SL form, and formulation and assessment of an alternative (the DS form).  
569 *Earth Surface Processes and Landforms* 32, 649–6714. doi:10.1002/esp.

570 Hack, J.T., 1957. *Studies of Longitudinal Stream Profiles in Virginia and Maryland*. U.S.  
571 *Geological Survey Professional Paper* 294-B, 97.

572 Harmar, O.P., Clifford, N.J., 2007. Geomorphological explanation of the long profile of the  
573 Lower Mississippi River. *Geomorphology* 84, 222-240.  
574 doi:10.1016/j.geomorph.2006.01.045.

575 Jassim, S. Z., Goff, J.C., 2006. *Geology of Iraq*, first ed. Dolin Prague and Moravian  
576 *Museum, Prague* (341pp).

577 Jones, R., 2002. Algorithms for using a DEM for mapping catchment areas of stream  
578 sediment samples. *Computers and Geosciences* 28, 1051-1060.

579 Keller, E., Pinter, N., 2002. *Active Tectonics: Earthquakes, Uplift, and Landscape*. Prentice  
580 *Hall, New Jersey*.

581 Khadivi, S., Mouthereau, F., Larrasoaña, J.C., Vergés, J., Lacombe, O., Khademi, E.,  
582 Beamud, E., Melinte-Dobrinescu, M. and Suc, J.P., 2010. Magnetochronology of  
583 synorogenic Miocene foreland sediments in the Fars arc of the Zagros Folded Belt (SW

584 Iran). Basin Research 22,918-932.

585 Khadivi, S., Mouthereau, F., Barbarand, J., Adatte, T. and Lacombe, O., 2012. Constraints on  
586 palaeodrainage evolution induced by uplift and exhumation on the southern flank of the  
587 Zagros–Iranian Plateau. *Journal of the Geological Society* 169, 83-97.

588 Kirby, E., Whipple, K., 2001. Quantifying differential rock-uplift rates via stream profile  
589 analysis. *Geology* 29, 415-418.

590 Kirby, E., Whipple, K.X., Tang, W., Chen, Z., 2003. Distribution of active rock uplift along  
591 the eastern margin of the Tibetan plateau: inferences from bedrock river profiles. *Journal*  
592 *of Geophysical Research: Solid Earth* 108, 2217.  
593 <http://dx.doi.org/10.1029/2001JB000861>.

594 Kirby, E., Whipple, K.X., 2012. Expression of active tectonics in erosional landscapes. *Journa*  
595 *of Structural Geology* 44, 54–75. doi:10.1016/j.jsg.2012.07.009.

596 Koshnaw, R.I., Horton, B.K., Stockli, D.F., Barber, D.E., Tamar-Agha, M.Y., Kendall, J.J.,  
597 2017. Neogene shortening and exhumation of the Zagros fold-thrust belt and foreland  
598 basin in the Kurdistan region of northern Iraq. *Tectonophysics* 694, 332–355.

599 Kottek, M., Grieser, J., Beck, C., Rudolf, B., Rubel, F., 2006. World Map of the Koppen-  
600 Geiger climate classification updated. *Meteorologische Zeitschrift* 15, 259–263.

601 Lacombe, O., Mouthereau, F., Kargar, S., Meyer, B., 2006. Late Cenozoic and modern stress  
602 fields in the western Fars (Iran): implications for the tectonic and kinematic evolution of  
603 central Zagros. *Tectonics* 25, TC1003. doi:10.1029/2005TC001831.

604 Lacombe, O., Bellahsen, N. and Mouthereau, F., 2011. Fracture patterns in the Zagros Simply  
605 Folded Belt (Fars, Iran): constraints on early collisional tectonic history and role of  
606 basement faults. *Geological Magazine* 148, 940-963.

607 Langbein, W. B. et al., 1947. Topographic characteristics of drainage basins. United States  
608 Geological Survey, W.-S. Paper 968-C, 125-157.

609 Larue, J.P., 2008. Effects of tectonics and lithology on long profiles of 16 rivers of the  
610 southern Central Massif border between the Aude and the Orb (France). *Geomorphology*  
611 93, 343–367. doi:10.1016/j.geomorph.2007.03.003.

612 Lavé, J., Avouac, J., 2000. Active folding of fluvial terraces across the Siwaliks Hills,  
613 Himalayas of central Nepal. *Journal of Geophysical Research* 105, 5735-5770.

614 Masson, F., Chery, J., Hatzfeld, D., Martinod, J., Vernant, P., Tavakoli, F., Ghafory-Ashtiani,  
615 M., 2005. Seismic versus aseismic deformation in Iran inferred from earthquakes and  
616 geodetic data. *Geophysical Journal International* 160, 217-226.

617 McQuarrie, N., 2004. Crustal scale geometry of the Zagros fold-thrust belt, Iran. *Journal of*

618           Structural Geology 26, 519–535.

619 McQuarrie, N., van Hinsbergen, D. 2013. Retrodeforming the Arabia-Eurasia collision zone:  
620           Age of collision versus magnitude of continental subduction. *Geology* 41, 315–318.  
621           doi:10.1130/G33591.1.

622 Miller, S.R., Baldwin, S.L., Fitzgerald, P.G., 2012. Transient fluvial incision and active  
623           surface uplift in the Woodlark Rift of eastern Papua New Guinea. *Lithosphere* 4, 131–  
624           149. doi:10.1130/L135.1.

625 Molin, P., Pazzaglia, F.J., Dramis, F., 2004. Geomorphic expression of active tectonics in a  
626           rapidly-deforming forearc, Sila massif, Calabria, southern Italy. *American Journal of*  
627           *Science* 304, 559-589.

628 Montgomery, D.R., Fournelle-Georgiou, E., 1994. Channel network source representation  
629           using digital elevation models. *Water Resources Research*. 29, 3925–3934.

630 Moosdorf, N., Cohen, S., von Hagke, C., 2018. A global erodibility index to represent  
631           sediment production potential of different rock types. *Applied Geography* 101, 36-44.

632 Morell, K.D., Kirby, E., Fisher, D.M., Van Soest, M., 2012. Geomorphic and exhumational  
633           response of the Central American Volcanic Arc to Cocos Ridge subduction. *Journal of*  
634           *Geophysical Research: Solid Earth* 117. doi:10.1029/2011JB008969.

635 Mouthereau, F., Lacombe, O., Meyer, B., 2006. The Zagros folded belt (Fars, Iran):  
636           constraints from topography and critical wedge modelling. *Geophysical Journal*  
637           *International* 165, 336-356.

638 Mouthereau, F., Tensi, J., Bellahsen, N., Lacombe, O., De Boisgrollier, T., Kargar, S., 2007.  
639           Tertiary sequence of deformation in a thin-skinned/thick-skinned collision belt: The  
640           Zagros folded belt (Fars, Iran). *Tectonics* 26, Tc5006, doi: 10.1029/2007tc002098.

641 Mouthereau, F., Lacombe, O., Vergés, J., 2012. Building the Zagros collisional orogen:  
642           timing, strain distribution and the dynamics of Arabia/Eurasia plate convergence.  
643           *Tectonophysics* 532, 27–60.

644 Nissen, E., Tatar, M., Jackson, J.A., Allen, M.B., 2011. New views on earthquake faulting in  
645           the Zagros fold-and-thrust belt of Iran. *Geophysical Journal International* 186, 928–944.

646 Obaid, A., Allen, M.B., 2017. Landscape maturity, fold growth sequence and structural style  
647           in the Kirkuk Embayment of the Zagros, northern Iraq. *Tectonophysics* 717, 27–40.

648 Olivetti, V., Cyr, A.J., Molin, P., Faccenna, C., Granger, D.E., 2012. Uplift history of the Sila  
649           Massif, southern Italy, deciphered from cosmogenic <sup>10</sup>Be erosion rates and river  
650           longitudinal profile analysis. *Tectonics* 31, 1–19, doi:10.1029/2011TC003037.

651 Perotti, C., Chiariatti, L., Bresciani, I., Cattaneo, L., Toscani, G., 2016. Evolution and timing

652 of salt diapirism in the Iranian sector of the Persian Gulf. *Tectonophysics* 679, 180–198.

653 Phillips, J.D., Lutz, J.D., 2008. Profile convexities in bedrock and alluvial streams.

654 *Geomorphology* 102, 554–566, doi:10.1016/j.geomorph.2008.05.042.

655 Pike, R. J., Wilson, S. E., 1971. Elevation-relief ratio, hypsometric integral, and

656 geomorphic area-altitude analysis. *Bulletin of the Geological Society of America* 82,

657 1079–1084.

658 Ramsey, L. A., Walker, T., Jackson, J., 2008. Fold evolution and drainage development in the

659 Zagros mountains of Fars province, SE Iran. *Basin Research* 20, 23–48.

660 Ruh, J.B., Hirt, A.M., Burg, J.P., Mohammadi, A., 2014. Forward propagation of the Zagros

661 Simply Folded Belt constrained from magnetostratigraphy of growth strata. *Tectonics*

662 33, 1534-1551.

663 Schildgen, T.F., Cosentino, D., Bookhagen, B., Niedermann, S., Yildirim, C., Echtler, H.,

664 Wittmann, H., Strecker, M.R., 2012. Multi-phased uplift of the southern margin of the

665 Central Anatolian plateau, Turkey: A record of tectonic and upper mantle processes.

666 *Earth and Planetary Science Letters* 317–318, 85–95. doi:10.1016/j.epsl.2011.12.003.

667 Schumm, S.A., 1956. Evolution of drainage systems and slopes in badlands at Perth Amboy,

668 New Jersey. *Bulletin of the Geological Society of America* 67, 597–646.

669 Schwanghart, W. and Scherler, D., 2014. TopoToolbox 2–MATLAB-based software for

670 topographic analysis and modeling in Earth surface sciences. *Earth Surface Dynamics* 2,

671 1-7.

672 Scotti, V.N., Molin, P., Faccenna, C., Soligo, M. and Casas-Sainz, A., 2014. The influence of

673 surface and tectonic processes on landscape evolution of the Iberian Chain (Spain):

674 Quantitative geomorphological analysis and geochronology. *Geomorphology* 206, 37-57.

675 Seeber, L., Gornitz, V., 1983. River profiles along the Himalayan arc as indicators of active

676 tectonics. *Tectonophysics* 92, 335341–337367.

677 Shahzad, F., Gloaguen, R., 2011. TecDEM: A MATLAB based toolbox for tectonic

678 geomorphology, part 1: drainage network preprocessing and stream profile analysis.

679 *Computers and Geosciences* 37, 250–260.

680 Sissakian, V.K., 2000. Geological Map of Iraq, Geological Survey and Mining, Baghdad,

681 Iraq, Scale 1:1,000,000.

682 Stern, R. J., Johnson, P., 2010. Continental lithosphere of the Arabian Plate: A geologic,

683 petrologic, and geophysical synthesis. *Earth-Science Reviews* 101, 29–67.

684 Strahler, A., 1952. Hypsometric (area-altitude) analysis of erosional topology. *Bulletin of the*

685 *Geological Society of America* 63, 1117–1142.

686 Snyder, N.P., Whipple, K.X., Tucker, G.E., Merritts, D.J., 2000. Stream profiles in the  
687 Mendocino triple junction region, northern California. *Bulletin of the Geological Society*  
688 of America 112, 1250–1263. doi:10.1130/0016-7606(2000)112<1250:lrrtfd>2.3.co;2.

689 Talbot, C.J., Alavi, M., 1996. The past of a future syntaxis across the Zagros, in Alsop. In:  
690 Alsop, G.I., Blundell, D.J., Davison, I. (Eds.), *Salt Tectonics*. Geological Society,  
691 London, Special Publications, 100, pp. 89–109. doi:10.1144/GSL.SP.1996.100.01.08. 1.

692 Talebian, M., Jackson, J., 2004. A reappraisal of earthquake focal mechanisms and active  
693 shortening in the Zagros mountains of Iran. *Geophysical Journal International* 156, 506–  
694 526.

695 Tucker, G.E., Whipple, K.X., 2002. Topographic outcomes predicted by stream erosion  
696 models: sensitivity analysis and inter-model comparison. *Journal of Geophysical*  
697 *Research: Solid Earth* 107, doi: 10.1029/2001JB000162.

698 Vergés, J., Saura, E., Casciello, E., Fernandez, M., Villasenor, A., Jimenez-Mount, I., Garcia-  
699 Castellanos, D., 2011. Crustal-scale cross-sections across the NW Zagros belt:  
700 implications for the Arabian margin reconstruction. *Geological Magazine* 148, 739–761.

701 Vernant, P., Nilforoushan, F., Hatzfel, D., Abbassi, M. R., Vigny, C., Masson, F., Nankali,  
702 H., Matinod, J., Ashtiani, A., Bayer, R., Tavakoli, F., Chery, J., 2004. Present-day crustal  
703 deformation and plate kinematics in the Middle East constrained by GPS measurements  
704 in Iran and northern Oman. *Geophysical Journal International* 157, 381–398.

705 Walcott, R., Summerfield, M., 2008. Scale dependence of hypsometric integrals: An analysis  
706 of southeast African basins. *Geomorphology* 96, 174–186.

707 Walker, R. T., Ramsey, L. A., Jackson, J., 2011. Geomorphic evidence for ancestral drainage  
708 patterns in the Zagros Simple Folded Zone and growth of the Iranian plateau. *Geological*  
709 *Magazine* 148, 901-910.

710 Whipple, K.X., Tucker, G.E., 1999. Dynamics of the stream-power river incision model:  
711 Implications for height limits of mountain ranges, landscape response timescales, and  
712 research needs. *Journal of Geophysical Research* 104, 17,661–17,674.

713 Whipple, K.X., Tucker, G.E., 2002. Implications of sediment-flux dependent river incision  
714 models for landscape evolution. *Journal of Geophysical Research* 107 (B2), doi:  
715 10.1029/2000JB000044.

716 Whipple, K.X., 2004. Bedrock Rivers and the Geomorphology of Active Orogens. *Annual*  
717 *Review of Earth Planetary Science* 32, 151–185.

718 Whittaker, A.C., Cowie, P. A., Attal, M., Tucker, G. E., Roberts, G. P., 2007. Contrasting  
719 transient and steady-state rivers crossing active normal faults: new field observations

720 from the Central Apennines, Italy. *Basin Research* 19, 529–556.

721 Whittaker, A.C., Attal, M., Cowie, P. A., Tucker, G. E., Roberts, G., 2008. Decoding temporal  
722 and spatial patterns of fault uplift using transient river long profiles. *Geomorphology*  
723 100, 506–526.

724 Whittaker, A.C., Boulton, S.J., 2012. Tectonic and climatic controls on knickpoint retreat  
725 rates and landscape response times. *Journal of Geophysical Research: Earth Surface*  
726 117, F02024.

727 Wobus, C.W., Hodges, K. V., Whipple, K.X., 2003. Has focused denudation sustained active  
728 thrusting at the Himalayan topographic front? *Geology* 31, 861–864.

729 Wobus, C., Whipple, K.X., Kirby, E., Snyder, N., Johnson, J., Spyropolou, K., Crosby, B.,  
730 Sheehan, D., 2006 . Tectonics from topography: procedurses, promise, and pitfalls.  
731 *Special papers-Geological Society of America* 398, 55–74. doi:10.1130/2006.2398(04).

732 Wohl, E. E., Merritt, D. M., 2001. Bedrock channel morphology. *Geological Society of*  
733 *America Bulletin* 113, 1205–1212.

734 Zebari, M.M. and Burberry, C.M., 2015. 4-D evolution of anticlines and implications for  
735 hydrocarbon exploration within the Zagros Fold-Thrust Belt, Kurdistan Region, Iraq.  
736 *GeoArabia* 20, 161-188.

737 Zielke, O., Arrowsmith, J.R., Ludwig, L.G., Akçiz, S.O., 2010. Slip in the 1857 and earlier  
738 large earthquakes along the Carrizo Plain, San Andreas Fault. *Science* 327, 1119-1122.

739